Title

Isomorphic Fluorescent Nucleoside Analogs

ISBN

9789811997754

Authors

Steinbuch, Kfir B

Tor, Yitzhak

Publication Date

2023

DOI

10.1007/978-981-19-9776-1_17

Isomorphic Fluorescent Nucleoside Analogs

Kfir B. Steinbuch and Yitzhak Tor

Contents

Abstract

Characterized by their high structural similarity to their native counterparts, yet endowed with useful photophysical features, isomorphic fluorescent nucleosides present enormous opportunities. Here we discuss their fundamental design features, compare and contrast them to other families of fluorescent nucleoside analogs, as well as illustrate their utility and highlight potential limitations. The isomorphic nature of the analogs and their faithful representation of the canonical nucleosides enable their enzymatic, sequence-specific incorporation into RNA and DNA oligonucleotides, typically resulting in minimal structural perturbations. Their photophysical responsiveness, signaling changes in their microenvironment, can therefore be exploited for biophysical and biochemical applications, and expanded to high-throughput screening settings. The chapter specifically illustrates their application for fluorescently monitoring metabolically relevant enzymatic reactions involving nucleobases, nucleosides, cofactors, and oligonucleotides, as well as their utilization for biophysically studying folding and recognition of RNA and DNA oligonucleotides. Focusing on two families of

K. B. Steinbuch · Y. Tor (✉)
Department of Chemistry & Biochemistry, University of California, San Diego, CA, USA
e-mail: kbsteinbuch@ucsd.edu; ytor@ucsd.edu

N. Sugimoto (ed.), *Handbook of Chemical Biology of Nucleic Acids*,
https://doi.org/10.1007/978-981-16-1313-5_17-1

fluorescent nucleoside analogs built upon thieno [3,4-*d*] pyrimidines and isothiazolo [4,3-*d*]-pyrimidines, which differ from one another by a single N atom, we further illustrate their utility as mechanistic probes, providing insight into the tolerance of diverse enzymes to minimal structural perturbations.

Keywords

Fluorescence · Nucleobases · Nucleosides · Nucleotides · Oligonucleotides · Cofactors · Assays

Introduction

The virtually non-emissive nature of the canonical nucleobases has led to the development of numerous fluorescent analogs to study the structure, functions, and dynamics of their cellular constituents (Crespo-Hernández et al. 2004; Sinkeldam et al. 2010; Gustavsson and Markovitsi 2021). Additionally, such tools can facilitate the development of screening assays, as fluorescence spectroscopy is a highly sensitive and information-rich technique (Dziuba 2022). To date, hundreds of fluorescent nucleobase analogs have been reported and are commonly classified according to their structural features as extended-, expanded-, pteridine-like, and isomorphic, among other classifications (Saito and Hudson 2018). The structure, which grants the analog its emissive nature, would often dictate its utility and application landscape (Xu et al. 2017).

Extended nucleobase analogs commonly attach a chromophore to the nucleobase directly or through a linker. The resulting modified nucleosides can normally maintain their Watson-Crick face, possess high emission quantum yields (QYs), and emit at longer wavelengths than those of naturally occurring fluorescent compounds found in biological systems (Saito and Hudson 2018). When the chromophore is conjugated to the π-system of the nucleobase, such as in the case of ^{DAB}G (Fig. 1a) (Saito et al. 2011), it would usually respond to changes in its microenvironment; however when incorporated into an oligonucleotide this response could result in quenching, as for the case of A^{p} (Fig. 1a), which has a QY of 0.73 in methanol, but a substantial drop in QY is observed when incorporated in a DNA strand (Young et al. 2005). A chromophore attached through a linker such as Cy5–4-dU would normally not respond to such changes and maintain its QY (Fig. 1a) (Yu et al. 1994). Extended nucleobase analogs are usually bulky, and frequently exceed the size of the nucleobases themselves. This usually prevents the use of such analogs in monitoring enzymatic reactions of nucleobases or free nucleosides, as their steric bulk tends to abolish their binding. Such analogs can potentially be used in oligomeric constructs, where their perturbation might be diminished or be of minimal consequences (Wilson and Kool 2006).

Expanded nucleobase analogs contain additional aromatic rings fused to the purine or pyrimidine core structure in positions that, ideally, do not perturb base pairing. The expanded conjugated aromatic system typically endows these analogs

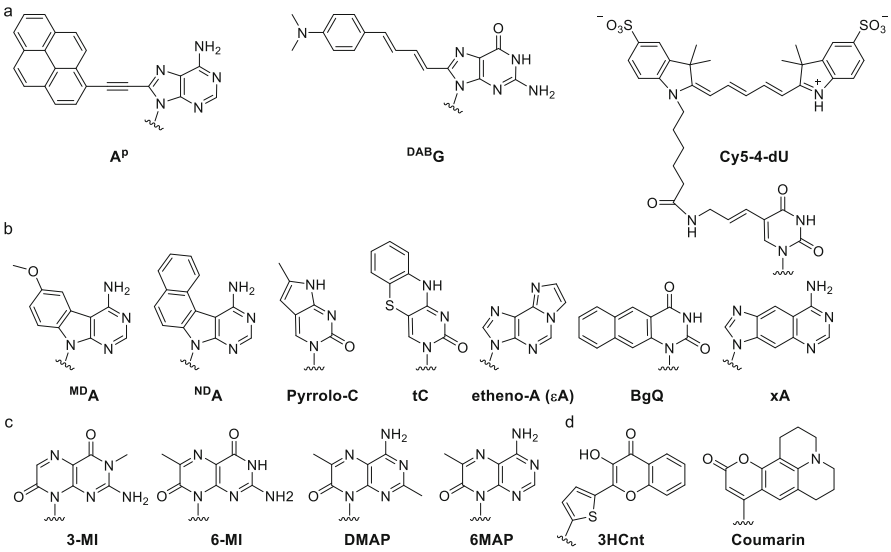

Fig. 1 Fluorescent nucleoside analogs. (**a**) Extended-, (**b**) expanded-, (**c**) pteridine-like, and (**d**) chromophoric analogs

with useful photophysical features. The emission of these analogs is also red-shifted in comparison to fluorescent cellular components, and their QYs could be high as in the case of BgQ (0.82) (Godde et al. 1998) but are normally somewhat lower as for the case of xA, etheno-A, pyrrolo-C, and tC with QYs between 0.17 and 0.5 (Fig. 1b) (Secrist et al. 1972; Leonard et al. 1976; Engman et al. 2004; Hardman et al. 2008). Notably, the expansion of the aromatic core does not guarantee higher QYs as such modifications could also facilitate non-radiative relaxation pathways, resulting in QY lower than 0.12 (Fig. 1b; ^{MD}A, ^{ND}A) (Okamoto et al. 2003, 2004). The structural enlargement of these analogs would also likely prevent the recognition by enzymes that act on the free nucleosides or nucleobases. While potentially less perturbing, these analogs might still impact the overall structure of their construct.

Pteridines can be placed somewhere between the expanded and isomorphic analogs as they contain a fused pyrazine ring onto the pyrimidine core, thus potentially mimicking purines. The most studied analogs are the guanosine-like 3-MI and 6-MI, which include methyl groups at perturbing and non-perturbing positions, respectively, as well as the adenosine mimics DMAP and 6MAP (Fig. 1c) (Hawkins 2001). These analogs are highly emissive and have been extensively utilized, mainly within oligonucleotide constructs. Incorporation of the perturbing methylated analogs can result, however, in destabilization as they cannot form Watson-Crick-like pairs.

An additional class of fluorescent nucleoside analogs, often referred to as chromophoric analogs, includes a complete replacement of the native heterocycle with an aromatic chromophore. These analogs do not maintain their Watson-Crick face and cannot be recognized by enzymes that process the native nucleosides. However, due

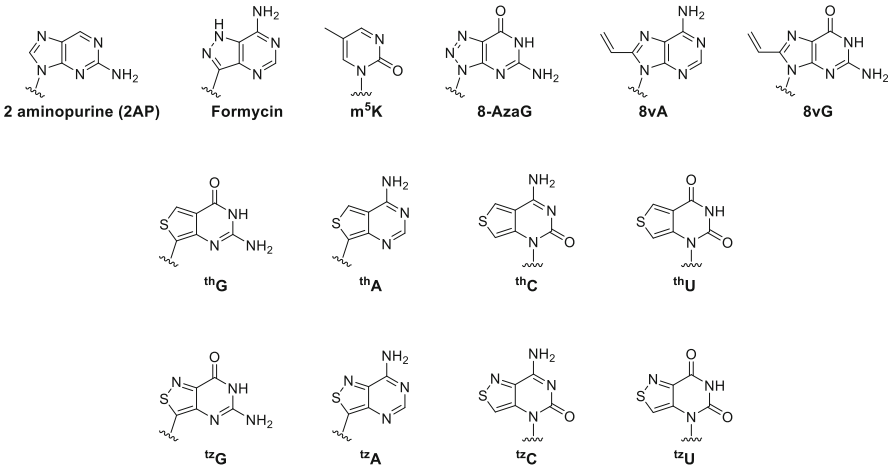

Fig. 2 Isomorphic fluorescent nucleoside analogs

to their extended π-system, these analogs often exhibit strong aromatic–aromatic interactions. Different chromophores with varying photophysical properties have been utilized for this purpose. Two examples include 2-thienyl-3-hydroxychromone nucleoside (3HCnt) a relatively small analog which will be discussed later in this chapter, and coumarin-based nucleobase analogs (Fig. 1d) (Coleman and Madaras 1998; Dziuba et al. 2012).

Isomorphic nucleoside analogs aspire to resemble the native nucleobases and minimize structural perturbations (Fig. 2) (Shin et al. 2011). The precise definition of what is considered isomorphic is evolving as the field advances. Analogs such as pyrrolo-C or 5-(Thien-2-yl)-2′-deoxyuridine were previously considered isomorphic, but today these are typically classified as expanded and extended analogs, respectively (Sinkeldam et al. 2010). Structural isomorphicity is desired to minimize the functional perturbations that accompany the chemical modifications, which can ultimately lead to "isofunctionality" (Rovira et al. 2017a). Nevertheless, this assessment has to be done on a case-by-case fashion, as chemical "deviations" in the analog's from the native structure will likely be tolerated differently in distinct biological applications (Rovira et al. 2015).

Isomorphicity frequently comes with a price, however, as the photophysical properties of many of these analogs are less than ideal. The absorption and emission wavelengths could be much shorter than those of the other categories, as in the case of 8-AzaG, formycin, m^5K, and others (Fig. 2) (Da Costa et al. 2007; Tor et al. 2007; Wierzchowski et al. 2014). 2-aminopurine (2AP), however, is an example of an analog that displays a high QY of 0.68 despite its small structure, and reviews describe its implementation (Fig. 2) (Rist and Marino 2002; Wilhelmsson 2010; Jones and Neely 2015). 8vA and 8vG, which are sometimes considered to be extended as they possess a vinyl group on adenosine and guanine 8-position (Fig. 2), respectively, also show high QYs (0.66 and 0.72, respectively) (Gaied

et al. 2005; Martinez-Fernandez et al. 2020). The thiopheno-based analogs shown in Fig. 2 also maintain good QYs (0.21–0.46) as well as red-shifted excitation and emission maxima (Shin et al. 2011). The isothiazolo family, however, while maintaining red-shifted excitation and emission maxima (Fig. 2), suffer from lower QYs (0.01–0.05 for the C U and A analogs, while the G analog maintain a good QY of 0.25) (Rovira et al. 2015). Within these two families, the cytosine and the uridine analogs could also be classified as expanded nucleobase analogs since the thiophene and izothiazole rings are fused to the pyrimidine core (Fig. 2).

Isomorphic nucleoside analogs have so far been used mostly in vitro. They are well tolerated by diverse enzymes, and they also serve as excellent replacements for the canonical ones in DNA and RNA oligonucleotides. Their inherent fluorescence is sensitive to their microenvironment; hence, they can serve as useful probes for structural changes and binding events. We refer to this microenvironmental sensitivity of photophysical properties as "responsiveness."

This chapter illustrates applications of isomorphic emissive analogs and the advantages associated with their use. Examples include monitoring enzymatic reactions of nucleobases and nucleosides, enzymatic reactions involving cofactors, utilization of isomorphic analogs within RNA and DNA oligonucleotides, enzymatic reactions on oligonucleotides, and ligand and protein binding to oligonucleotides. The chapter will focus mainly on the applications of the thiopheno- and isothiazolo-based analogs reported by our laboratory. Using nucleoside surrogates so close in structure to the native ones frequently also provides mechanistic insight, as discussed. A better understanding of these analogs and the type of questions they can help answer will facilitate their further implementation and could perhaps inspire the fabrication and implementation of the next generation of isomorphic fluorescent nucleosides.

Enzymatic Reactions of Nucleosides and Nucleobases

Enzymes responsible for metabolizing and utilizing nucleoside and nucleotide are typically substrate-specific, thus limiting the use of most fluorescent analogs in monitoring their reactions (Sinkeldam et al. 2013). Isomorphic emissive surrogates, specifically the thieno- and isothiazolo-based analogs, present, however, a viable approach to optically monitoring such processes, as they are frequently well tolerated. Several examples, demonstrating the use of isomorphic nucleoside analogs to monitor enzymatic reactions, are discussed in this section, including the deamination reactions of adenosine, cytidine, and guanine as well as the dealkylation of guanine (Sinkeldam et al. 2013; Rovira et al. 2015; Ludford et al. 2019, 2021; Adamek et al. 2020; Bucardo et al. 2021; Fillion et al. 2022). These examples highlight their utility for real-time fluorescence-based monitoring of enzyme-mediated reactions and illustrate their potential for assembling high-throughput screens to discover new therapeutics.

Adenosine-, cytidine-, and guanine deaminases, commonly referred to as ADA, CDA, and GDA, respectively, serve important roles in regulating the cellular

concentration of their respective substrates. Insufficient or elevated activities of these enzymes are frequently associated with pathological disorders. ADA inhibitors are in clinical use for treating leukemia and lymphomas (Adamek et al. 2020). CDA deaminates several prodrugs used in chemotherapy but is also known to deaminate several chemotherapeutic drugs, thus diminishing their effectiveness (Micozzi et al. 2014; Ludford et al. 2021). Human GDA was recently found to take part in regulating neurological conditions such as traumatic brain injury and psychiatric disorders. Perhaps due to its high degree of substrate specificity, the study of human GDA appears limited in comparison to other deaminases (Bucardo et al. 2021). Studying these enzymes and developing methods to readily and reliably monitor their activity and inhibition is therefore of great importance.

Current methods for analyzing deaminases include, among others, chromatographic methods or absorption spectroscopy. The former requires relatively large quantities and are not normally amendable for high-throughput formats, while the latter is potentially suitable for such applications. However, since most candidate inhibitors are substrate- or transition state-analogs, they share a chromophoric skeleton with the nucleosides/nucleobase substrate and thus typically absorb in the same UV range. This optical interference hampers monitoring these reactions in the presence of potential inhibitors. The use of the thiopheno- and izothiazolo-isomorphic fluorescent analogs thus opens an optical window, facilitating the monitoring of these reactions in longer wavelengths, minimizing interference from potential inhibitors. Firstly, the absorption spectra of these isomorphic analogs are red-shifted in comparison to the native substrates; less interference is therefore expected from potential inhibitors when monitoring these reactions. Secondly, their visible range emission typically circumvents this interference, minimizing interference by protein residues or other low MW fluorescent components (which typically emit in the UV). Finally, since the analogs undergo a deamination reaction, they yield new chromophores with distinct photophysics (Sinkeldam et al. 2013; Rovira et al. 2015; Ludford et al. 2019, 2021; Adamek et al. 2020; Bucardo et al. 2021).

ADA deaminates adenosine to inosine (Fig. 3a). The emissive surrogates thA and ^{tz}A were both found to be compatible substrates and both facilitated the monitoring of the reaction by either fluorescence or absorbance (Fig. 3b) (Sinkeldam et al. 2013; Rovira et al. 2015; Ludford et al. 2019; Adamek et al. 2020). Kinetic parameters demonstrate that ^{tz}A reacts almost identically to adenosine to form the emissive ^{tz}I, while thA reacts slower to form thI (Ludford et al. 2019). This provided insight into the importance of the substrate's N7 nitrogen, which is supported by crystallographic studies showing a hydrogen bond to adenosine's N7 in the active site (Ludford et al. 2019). Differences in the photophysics of ^{tz}A and thA and their respective inosine derivatives, as well as differences in their enzyme binding affinities, provide distinct spectral windows for reaction monitoring and over different time spans. These features were exploited for the fabrication of inhibitor discovery assays (Sinkeldam et al. 2013; Ludford et al. 2019). ^{tz}A was further utilized, in a high-throughput format, to screen a library of ~350 potential inhibitors, where a promising new scaffold for ADA inhibitors was found (Adamek et al. 2020; Ludford and Tor 2020).

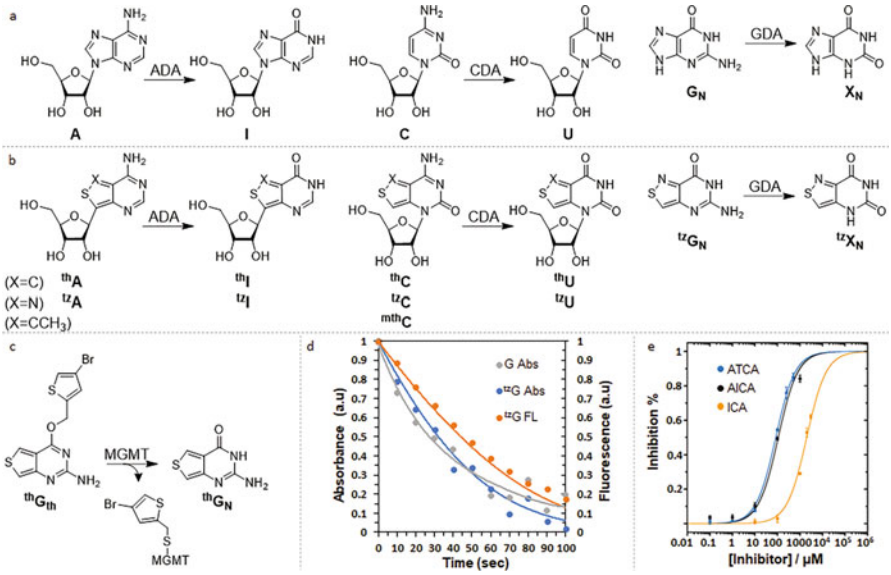

Fig. 3 Deamination reactions by ADA CDA and GDA of native (**a**) and emissive (**b**) nucleosides and nucleobases. (**c**) Dealkylation of $^{th}G_{th}$ by MGMT releases the emissive $^{th}G_N$. (**d**) Absorbance of G, and absorbance and emission of ^{tz}G during GDA reaction over time. (**e**) ^{tz}G-fluorescence-based GDA-inhibitor screening

CDA deaminates cytidine to uridine (Fig. 3a). ^{th}C, ^{tz}C, as well as the recently reported ^{mth}C (a member of a newly published emissive alphabet) (Ludford et al. 2022) were all found to be suitable CDA substrates, and deamination was monitored by absorbance and fluorescence (Fig. 3b) (Ludford et al. 2021). Screening for inhibitors was also facilitated by the three analogs. Most intriguing, however, was the kinetic analysis, which shed light on the enzyme's active site. Analyses suggested that the fusion of the five-membered isothiazolo- or thiopheno-ring onto the pyrimidine ring could potentially enhance binding, while the addition of the methyl group (as in ^{mth}C) slightly weakened it. The analysis also showed accelerated deamination and unbinding rates for the ^{th}C and ^{mth}C analogs, indicating some tolerance to steric perturbations (Ludford et al. 2021).

GDA deaminates guanine to xanthine (Fig. 3a). The lack of the rather large and contact-forming D-ribose presents a challenge in the search for a reporting surrogate as any alteration to the nucleobase might be detrimental. Both $^{th}G_N$ and $^{tz}G_N$ were thus examined as potential GDA substrates (Fig. 3b). $^{tz}G_N$ was found to react very similarly to guanine with comparable kinetic parameters, while $^{th}G_N$ did not undergo any deamination, suggesting the importance of the purine's N7 to the substrate's recognition (Fig. 3d). This was further supported by molecular docking experiments (MOEs) that suggested hydrogen bonding to the N7 of guanine. As for ADA and CDA, the conversion of $^{tz}G_N$ to $^{tz}X_N$ facilitated real-time reaction monitoring using either absorbance or fluorescence and was utilized for inhibitor screening of two

newly synthesized compounds, 4-aminoisothiazole-3-carboxamide (ATCA) and 4-imidazolecarboxylic acid (ICA) as well as the established competitive GDA inhibitor, 5-aminoimidazole-4-carboxamide (AICA) (Fig. 3e) (Bucardo et al. 2021).

Finally, another example for the application of isomorphic nucleobases to monitor enzymatic reactions is using $^{th}G_N$ (Fig. 3c) to fluorescently monitor the reaction of O^6-methylguanine-DNA-methyltransferase (MGMT) (Fillion et al. 2022). This enzyme facilitates a key DNA repair process that removes alkyl residues from O^6-alkylated guanines through an irreversible reaction, yielding a deactivated alkylated enzyme and guanine. This repair pathway can interfere, however, with anticancer treatment, as chemotherapeutic drugs such as Temozolomide and Carmustine, used for the treatment of glioblastoma, exert their cytotoxic effect by alkylating G residues (which, when uninterrupted, ultimately leads to malfunctions in DNA replication and eventually to cell death). MGMT can thus diminish or even eliminate the cytotoxic effect of these drugs. As levels of MGMT can vary between patients, determining MGMT Levels is key to projecting the potential efficacy of such treatments and therefore could be imperative for treatment strategy. In addition, inhibitors of MGMT can act as potential anticancer agents (Fillion et al. 2022).

Previous methods for assessing MGMT activity involved FRET-based oligonucleotide substrates, or probes based on O^6-benzylguanine conjugated to a fluorophore or a fluorophore–quencher pair as a pseudo-substrate. These methods could, however, be complex, requiring long reaction times due to the bulkiness of the alkyl group. The isomorphicity of $^{th}G_N$ and its inherent fluorescence enabled the attachment of small moieties that quench its emission, such as 3-iodobenzyl and 4-bromothenyl, yielding the analogs $^{th}G_I$ and $^{th}G_{th}$, respectively, which were found suitable for fluorescent monitoring of the reaction with MGMT in real-time. As perhaps expected, the less perturbing 4-bromothenyl group resulted in faster reaction times. A linear calibration curve of fluorescent intensities at a specific reaction time vs. concentration of MGMT was established, facilitating the determination of MGMT's activity levels. $^{th}G_{th}$ was also utilized to evaluate the inhibitory effect of a known inhibitor; illustrating this method is also potentially amendable for high-throughput screening applications (Fillion et al. 2022).

Enzymatic Reactions of Nucleobase-Based Cofactors

Nucleosides and nucleotides also participate in cellular pathways as cofactors and secondary messengers. Emissive surrogates for these small molecules are thus needed as biophysical and mechanistic tools (Rovira et al. 2017b). Similar to metabolic pathways, enzymes relying on such cofactors can also be substrate specific and sensitive to perturbations. Capitalizing on the thieno- and isothiazolo-based alphabets, the synthesis and biosynthesis of isomorphic emissive cofactors and their metabolic interconversions by transferases, kinases, and hydrolases have also been explored, and their ability to fluorescently monitor and study signaling and metabolic pathways has been demonstrated. Among the cofactors explored are ATP, NAD^+, NADH, $NADP^+$, NADPH, as well as cyclic dinucleotides (CDNs) –

secondary messengers produced mainly by bacteria (Rovira et al. 2017b; Hallé et al. 2018; Feldmann et al. 2019; Li et al. 2020b, a). The biosynthesis and isofunctionality of emissive cAMP and SAM analogs were also explored but will not be discussed here (Vranken et al. 2016).

NAD^+ and NADH, its corresponding reduced form, are key determinants of the cellular redox state (Navas and Carnero 2021). In addition, NAD^+ also serves as substrate for several key enzymes, including poly-ADP-ribose polymerases (PARPs), mono-ADPribose transferases (ARTs), sirtuins, cyclases, and DNA ligases (Rovira et al. 2017b). All these reactions involve the hydrolysis of the nicotinamide group. The participation of NAD^+ in metabolic and regulatory processes triggered the exploration of emissive analogs early on. A prominent fluorescent NAD^+ analog is the $1,N^6$-etheno NAD^+ (εNAD^+), which has been utilized in numerous biochemical assays for NAD^+-consuming enzymes (Barrio et al. 1972). Two traits of εNAD^+ limit its use, though. First, its extended structure abolished its Watson-Crick face and it is therefore somewhat perturbing. Secondly, it is internally quenched by its nicotinamide moiety, and a fluorescent signal is regenerated only upon cleavage of this heterocycle, thus limiting its applications (Rovira et al. 2017b).

A distinctive feature of NAD^+/NADH (and hence $NADP^+$/NADPH) among all other cofactors is that NADH is somewhat emissive while NAD^+ is not. Redox reactions interconverting the two could therefore be fluorescently monitored utilizing the native cofactors. Conversely, the enzymatic synthesis of NAD^+ or reactions including the cleavage of its nicotinamide moiety would not generate emissive entities (Hallé et al. 2018). The photophysical behavior of the isothiazolo and thieno NAD^+/NADH analogs ($N^{tz}AD^+$ and $N^{th}AD^+$, respectively) in redox-based reactions is complementary to that of the native cofactors, with a drop in fluorescence when the emissive NAD^+ is reduced to NADH. Additionally, since $N^{tz}AD^+$ and $N^{th}AD^+$ are intrinsically emissive, all the NAD^+-derived analogs are fluorescent as well; therefore all transfer reactions could be monitored (Fig. 4). The isofunctionality of the isomorphic NAD^+ analogs and their ability to fluorescently monitor enzymatic processes have been demonstrated using enzymes that represent diverse reactions, including the synthesis of NAD^+, redox-type reactions, and hydrolysis of the nicotinamide moiety (Rovira et al. 2017b; Feldmann et al. 2019).

The enzymatic syntheses of $N^{th}AD^+$ and $N^{tz}AD^+$ starting from their corresponding ATP analogs have been accomplished at preparative scales utilizing the commercially available nicotinamide adenylyl transferase 1 (NMNAT-1) as shown in Fig. 4. It was found advantageous as the chemical synthesis of NAD^+ analogs is frequently challenging, time-consuming, and low yielding (Hallé et al. 2018; Feldmann et al. 2019). Redox-type reactions were demonstrated utilizing *Saccharomyces cerviseae* alcohol dehydrogenase (ADH) and lactate dehydrogenase (LDH) (Rovira et al. 2017b; Hallé et al. 2018; Feldmann et al. 2019). Finally, cleavage reactions of the nicotinamide moiety were demonstrated utilizing porcine brain NADase, which hydrolyses the nicotinamide glycosidic bond to release ADP-ribose (ADPR), an important secondary messenger, Cholera toxin subunit A (CTA), an ART, and PARP1, a key regulatory enzyme (Rovira et al. 2017b; Hallé et al. 2018; Feldmann et al. 2019). The latter, PARP1, was an exception, as $N^{tz}AD^+$ was found to

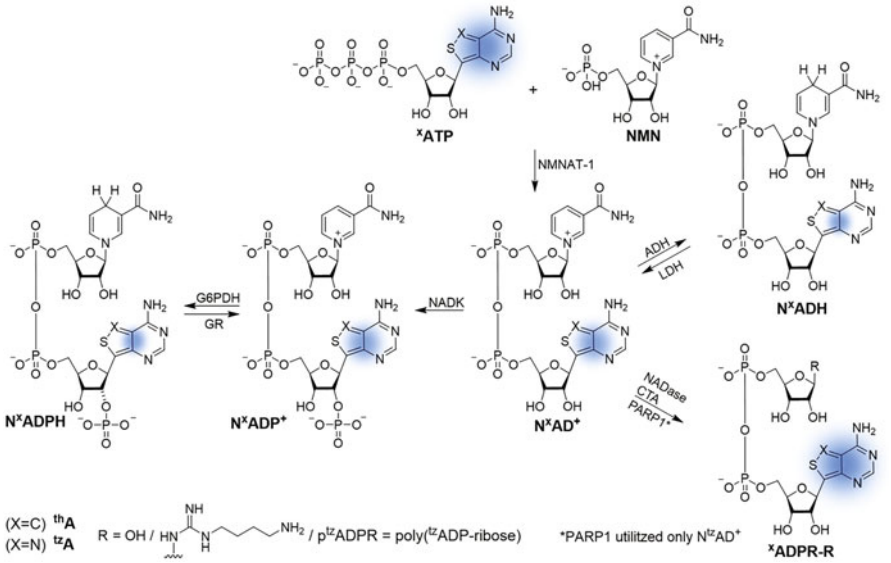

Fig. 4 Emissive NAD^+ and $NADP^+$ enzymatic synthesis and their reactions. NAD^+ analogs reactions include redox type reactions and hydrolysis of the nicotinamide moiety. All analogs are emissive; responsiveness of the ^{th}A and ^{tz}A moieties facilitates fluorescent monitoring of all reactions described

be processed to a lower extent in comparison to the native NAD^+ and $N^{th}AD^+$ was not accepted at all as a substrate (Fig. 4) (Feldmann et al. 2019).

The ^{th}A-based analogs have been found to be generally more responsive, providing a larger emission dynamic range, whereas the ^{tz}A-based analogs were found to be more functional, as conversion rates and reaction times were closer to those of the native cofactors. The different reactivity suggested, as before, the enzymes' dependency on the N7 nitrogen of the adenosine's imidazole ring. Crystallographic studies of NAD^+-bound PARP1 indeed indicated interactions between N7 and the protein. Intriguingly, the comparison between $N^{th}AD^+$ and $N^{tz}AD^+$ as CTA substrates suggested the importance of the N7 in substrate recognition, although crystallographic studies had not clearly revealed such contacts (Feldmann et al. 2019).

Isomorphic analogs of the NAD^+-related cofactor, $NADP^+$ and its reduced form NADPH, were also synthesized and explored utilizing ^{tz}A (Hallé et al. 2018). Intracellular levels of $NADP^+$ are much lower than those of NAD^+, and one of the key functions of $NADP^+$/NADPH in cells is in the antioxidant systems (Ying 2008). To showcase the utility of the ^{tz}A-based analogs, $N^{tz}ADP^+$ was synthesized from $N^{tz}AD^+$ by NAD^+ kinase (NADK) and ATP. The synthesis could not be monitored by fluorescence as the ribose phosphorylation does not measurably affect the compound's photophysical properties. Reduction by glucose 6 phosphate dehydrogenase (G6PDH) to $N^{tz}ADPH$ was accompanied, however, by a drop in fluorescence similar to $N^{tz}AD^+$/$N^{tz}ADH$. $N^{tz}ADPH$ was also used to monitor the reduction of

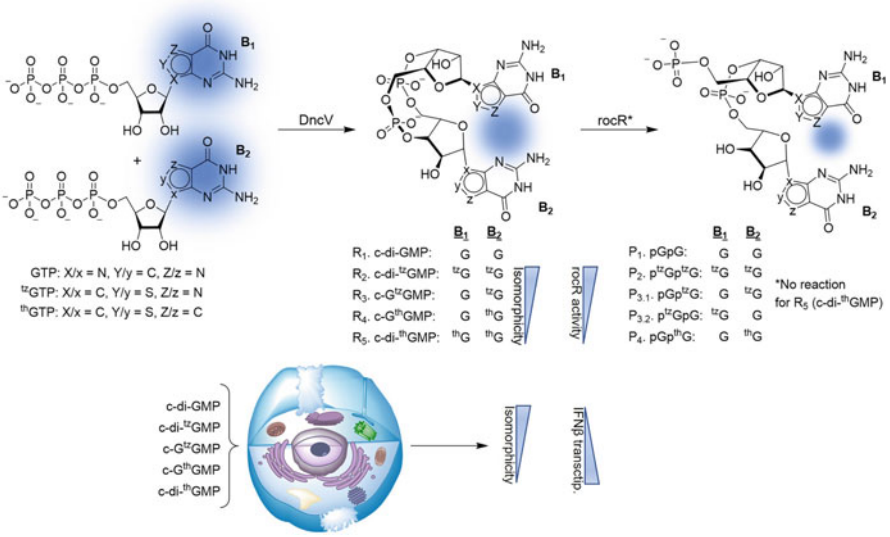

Fig. 5 Enzymatic synthesis and hydrolysis of native CDNs and analogs by DncV and rocR, respectively. Fluorescence intensity decreases with synthesis and hydrolysis. As isomorphicity level decreases, rocR activity decreases as well (top). Transfection of CDN analogs induces downstream immune response. As isomorphicity level decreases, higher levels of IFN-β transcription are observed (bottom)

oxidized glutathione (GSSG) to glutathione (GSH) by glutathione reductase (GR). As expected, an increase in fluorescence signal was observed, illustrating that this reaction could also be monitored by fluorescence. Notably, $N^{tz}ADP^{+}/N^{tz}ADPH$ displayed similar conversion rates to the native analogs (Fig. 4) (Hallé et al. 2018).

Finally, ^{th}GTP and ^{tz}GTP were used to fluorescently study the enzymatic synthesis and hydrolytic cleavage of CDNs, as well as their immunostimulatory effects in mammalian cells (Fig. 5) (Li et al. 2020b, a). As secondary messengers, CDNs regulate central processes in all bacteria, including motility, virulence, and biofilm formation. Multiple dinucleotide cyclases and phosphodiesterases (PDEs), which produce and hydrolyze the CDNs, respectively, tightly regulate their intracellular concentration. Bacterial CDNs are recognized as pathogen-associated molecular patterns (PAMPs) and trigger the innate immune response in eukaryotic cells. Pattern recognition receptors (PRRs) on the cell surface of eukaryotic cells or intracellular receptors detect such PAMPs, trigger the innate immune response, and further modulate the adaptive immune response. Fluorescent analogs can therefore be used to study and monitor the pathways involved in CDNs production, degradation, and recognition (Li et al. 2020b, a).

Vibrio cholerae's dinucleotide cyclase (DncV) and *P. aeruginosa*'s PDE rocR have been utilized for the in vitro synthesis and the hydrolysis of emissive CDN analogs, respectively. DncV produces the heterodimeric CDN 3′,3′-c-GAMP in vivo, but was reported to be promiscuous enough in vitro to also produce c-di-

GMP and c-di-AMP when provided with the respective purine nucleotides. thGTP and ^{tz}GTP were accepted by DncV and produced the corresponding symmetric CDN analogs c-di-thGMP and c-di-^{tz}GMP as well as the mixed analogs, c-G^{tz}GMP and c-GthGMP (Fig. 5). An expected, fluorescence decrease was observed in all cyclization reactions, as the two nucleobases stack in the product. Reaction times and yields of the symmetric CDN reactions decreased in the order c-di-GMP, c-di-^{tz}GMP, and finally c-di-thGMP. Uncyclized intermediates were more prominent in the slower reactions. The slower formation rates for the thG-containing derivatives, along with the accumulation of the uncyclized intermediates, highlight the importance of the donor N at the purine's 7 position for DncV's activity (Li et al. 2020b).

The PDE rocR is one of *P. aeruginosa*'s most active and well-studied PDEs. It contains an EAL domain and specifically recognizes and cleaves c-di-GMP into the linear dinucleotide pGpG. When a non-symmetrical CDN analog is hydrolyzed, though, two distinct products, pGpN and pNpG, can potentially form, which further provided an opportunity to compare and contrast the isomorphicity of ^{tz}G and thG. Interestingly, a gradually reduced hydrolysis rates were observed as the structures progressively deviated from the parent CDN: c-di-GMP, to c-G^{tz}GMP, c-di-^{tz}GMP, c-GthGMP, to no reaction for c-di-thGMP (Fig. 5). Even more intriguingly, two different cleavage products were observed for c-G^{tz}GMP, while only one was observed for the cleavage of c-GthGMP, demonstrating that both phosphodiester bonds are cleaved in the former while only one is selectively cleaved in the latter. These observations suggest that the lack of the purine N-7 has a detrimental role on rocR-mediated hydrolysis. The non-symmetric CDNs, c-G^{tz}GMP and c-GthGMP, facilitated fluorescence monitoring of the CDN cleavage reaction (Li et al. 2020b).

It is important to note that other fluorescent CDN analogs based on εA and 2AP were explored for fluorescent monitoring of the synthesis and degradation of CDNs; however, they could not be enzymatically synthesized. In addition, while monitoring PDE-mediated degradation was possible using the 2AP-based CDN analog, the fluorescence intensities of the εA-based CDN and the corresponding linear dinucleotide analogs were low, and hence of limited utility (Zhou et al. 2017).

Next, to examine the cellular activity of the new isomorphic emissive analogs in mammalian cells, their ability to induce an immune response via the "stimulator of interferon genes" (STING) pathway was evaluated (Li et al. 2020a). Two downstream reporters for STING activation were monitored upon transfection of the CDN analogs into murine cells, phosphorylated IRF3 (pIRF3, a transcription factor) and IFN-β (a type-I interferon). All analogs, except for c-di-thGMP, induced a cellular immune response detected by increased levels of both pIRF3 and IFN-β. In some cases, levels were considerably higher than those induced by the native c-di-GMP. The lack of activity of c-di-thGMP, however, suggests insufficient cellular recognition. IFN-β production shows that the peak response for c-G^{tz}GMP, c-di-^{tz}GMP, and c-GthGMP occurs sooner than for the native CDN. Intriguingly, the less isomorphic the analogs were, the levels of IFN-β transcription were further increased, suggesting longer cellular residency time that prolongs their effect (Fig. 5) (Li et al. 2020a).

A thG-based analog of the 2′,3′-cyclic guanosine monophosphate-adenosine monophosphate (2′,3’-cGAMP) was recently synthesized chemically. This CDN is normally produced in mammalian cells by the cyclic GMP-AMP synthase (cGAS) upon its recognition of free DNA in the cytoplasm, which indicates bacterial or viral infection. The CDN then induces an immune response via the STING pathway. Although considerably reduced in vitro affinity to human and murine STING was seen for the 2′,3’-cthGAMP in comparison to the native CDN, the thG-based analog still activated IRF3 in mammalian cells. Importantly, cellular uptake was confirmed by two-photon excitation fluorescence microscopy along with fluorescence lifetime measurements (Veth et al. 2022).

RNA and DNA Oligonucleotide Constructs

In the context of DNA and RNA oligonucleotides, structural perturbations introduced by expanded or extended analogs could be tolerated for certain applications (Okamoto et al. 2005; Dodd and Hudson 2009). For monitoring intricate structural changes of well-folded structures (e.g., ribozyme), ligand binding events, or enzymatic reactions, structural perturbations could skew the results (Dziuba et al. 2021). Minimally perturbing fluorescent nucleoside analogs, which serve as faithful surrogates of their native counterparts, thus present significant advantages (Mély et al. 2020). Several examples are discussed in this section, including the use of isomorphic nucleoside analogs to follow conformational changes (Park et al. 2014), binding events (Liu et al. 2013), enzymatic reactions (Mizrahi et al. 2015), base flipping (Kilin et al. 2017), and other processes in RNA and DNA oligonucleotides (Sholokh et al. 2015).

Notably, the high structural similarity of isomorphic fluorescent nucleosides facilitates their enzymatic introduction into oligonucleotides. thGTP was shown to initiate T7 RNA polymerase-mediated transcription and generate short and long RNA transcripts where all the guanosine residues were replaced by thG (Fig. 6a, top) (McCoy et al. 2014). To generate singly labeled RNA oligonucleotides, enforced transcription initiation with the nucleoside thG yields 5′-end labeled transcripts, which can be monophosphorylated and ligated to a second RNA strand, providing the desired full-length RNA strand (Fig. 6b, top). These syntheses illustrate the isofunctionality of thG, as it is accommodated by three distinct enzymes, a polymerase, a kinase, and a ligase (Li et al. 2017).

RNA Folding and Ribozyme Activity

The proper folding and function of fully thG-modified RNA transcripts were evaluated by exploring a modified ribozyme and its modified RNA substrate (McCoy et al. 2014). The selected minimal hammerhead ribozyme (HH16) is a 38-mer containing 13 guanosine residues, which cleaves its substrate RNA strand, a 17-mer containing five guanosine residues (Fig. 6a, bottom left) (Long and

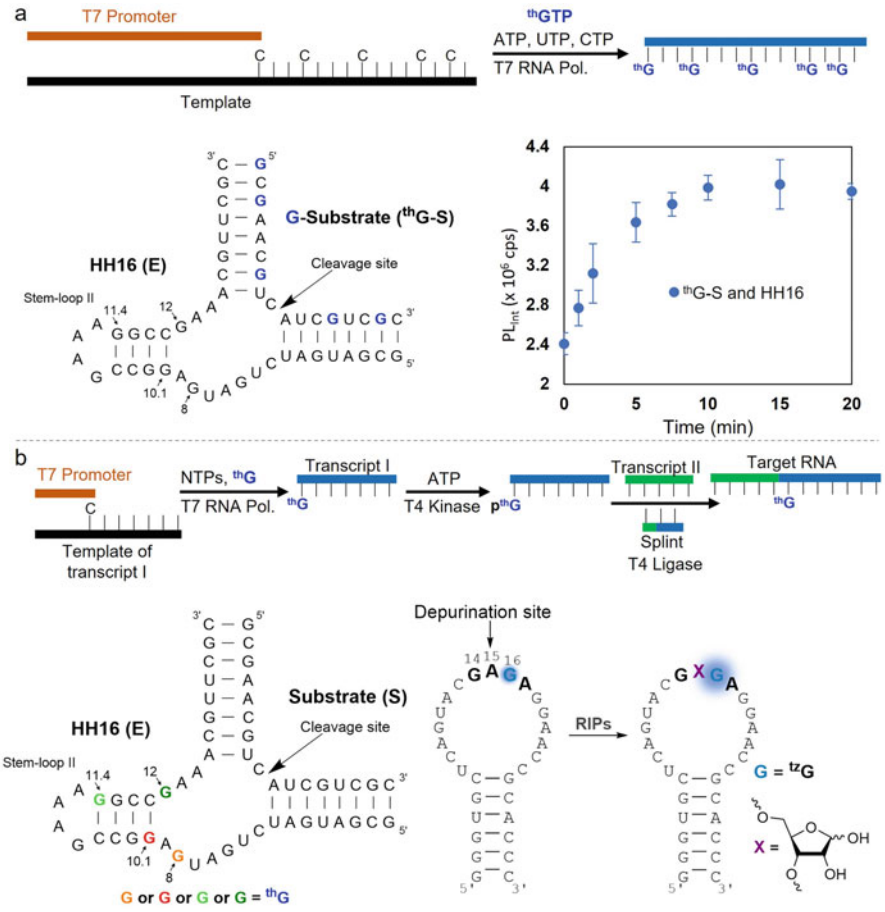

Fig. 6 Enzyme-mediated approaches for the assembly of fully thG-modified (**a**) and singly thG-modified (**b**) RNA transcripts and their utilization. (**a**) Hammerhead ribozyme-HH16 (E) and fully thG-modified substrate (bottom left); fluorescence intensity of the cleavage of thG-S by HH16 over time (bottom right). (**b**) G residues replaced in HH16 to form the four singly modified transcripts (bottom left); α-sarcin/ricin loop including the $^{(14)}$GAGA$^{(17)}$ tetraloop. Upon depurination of A15, fluorescence intensity of ^{tz}G at G16 increases

Uhlenbeck 1994). Native HH16 was shown to cleave the fully modified substrate (thG-S) at similar rates to the cleavage of the native substrate (S), suggesting similar hybridization and folding. Utilizing the emissive surrogate also facilitated the monitoring of the reaction using steady-state fluorescence spectroscopy (Fig. 6a, bottom right) (McCoy et al. 2014). Conversely, the fully modified HH16 (thG-E) showed very little cleavage ability of either substrate, stressing that catalytic RNA assemblies are exceedingly sensitive to even minute structural alterations (McCoy et al. 2014).

To showcase the use of singly thG-modified RNA oligonucleotides and to shed light on the observations mentioned above, four additional strands were constructed, each consisting of a single thG modification at residues previously found to be involved in catalysis: G8, G10.1, and G12, as well as in position 11.4, located at the stem-loop II, which is not in the catalytic center (Fig. 6b, bottom left) (Li et al. 2017). The strands $^{th}G_{10.1}$-E and $^{th}G_{12}$-E modified at the G10.1 and the G12 positions, respectively, performed as expected.

According to previous studies, G10.1 coordinates to divalent ions through its N7 nitrogen, thus explaining the very little activity $^{th}G_{10.1}$-E exhibited. Since G12 is proposed to assist in deprotonating the 2'-OH of C17, it was no surprise that $^{th}G_{12}$-E behaved very similarly to the native ribozyme, as thG and G display similar pK_a values. Interestingly, while it is proposed that only the ribose of G8 is involved in catalysis, $^{th}G_8$-E showed low enzymatic potency. The cause might be an impact on the tertiary WC base-pairing with the invariant C3. Finally, although G11.4 is not at the catalytic center, studies have shown that specific mutations at stem-loop II of HH ribozymes could improve cleavage rate, which perhaps explains the surprising increased cleavage activity demonstrated by $^{th}G_{11.4}$-E. The construction of singly thG-modified RNA strands has therefore provided, in addition to a fluorescence handle, a potential mechanistic insight into RNA folding and dynamics (Li et al. 2017). It would certainly be appealing to further explore these enzymatically active constructs using ^{tz}G, which includes the N7 nitrogen.

RNA/DNA–Protein Interactions

An emissive single G-modified RNA oligonucleotide was also utilized to fluorescently monitor the activity of ribosome-inactivating proteins (RIPs) (Cong et al. 2022). These highly cytotoxic proteins, which are prevalent among plants, fungi, and bacteria, irreversibly interfere with protein synthesis by depurinating a specific adenosine residue within the conserved α-sarcin/ricin loop of eukaryotic ribosomal RNA. In addition to being of interest as biological warfare agents, certain RIPs have been promoted as potential therapeutic tools (Cong et al. 2022).

^{tz}G was judiciously introduced next to the depurination target, the adenosine 15 residue (A15), which is a part of the $^{(14)}$GAGA$^{(17)}$ sequence tetraloop of the α-sarcin/ricin loop (Fig. 6b, bottom right). The susceptible adenosine residue could not obviously have been replaced with the thieno or izothiazolo adenosine isomorphic analogs since these are C-nucleosides. Prior structural studies indicated that G16 was properly oriented and stacked on A15 but G14 was not. This suggested the former should experience the largest depurination-induced environmental change. Additionally, a hydrogen bonding involving G16's N7 suggests this nitrogen may be important for maintaining the constrained loop structure. These observations and hypotheses thus suggested that replacing G16 with ^{tz}G may facilitate fluorescence monitoring of A15 depurination (Cong et al. 2022).

The fluorescent ^{tz}G16-containing α-sarcin/ricin loop was shown to depurinate at the same position as the native substrate RNA, albeit slower. An increase in

fluorescence signal was observed with reaction progress, as anticipated, due to depurination of the stacked adenosine and greater solvent exposure (Fig. 6b, bottom right). An RNA strand where the G14 was replaced by ^{tz}G was also susceptible to depurination; however, this reaction could not be fluorescently monitored, as predicted. Interestingly, the RNA substrate with thG replacing G16 was also susceptible to depurination. Reaction occurred, however, at a different site, suggesting that the lack of the N7 nitrogen altered the RNA secondary structure (Cong et al. 2022).

Protein/RNA interaction monitoring was also facilitated by utilizing the isomorphic adenosine analog, thA, as it was used to fluorescently monitor the enzymatic reaction of human adenosine deaminase acting on RNA 2 (hADAR2) (Mizrahi et al. 2015). ADARs, similar to ADA, deaminate adenosine to form inosine (which is then interpreted downstream as "G"); however ADARs function in the context of double-helical RNA structure. Unlike ADAs, the reaction rate of hADAR2 is not as dependent on the presence of the purine's N7 nitrogen. Similar reaction rate constants were obtained for deamination of the native and thA-containing mRNA sequences, establishing thA as a compatible adenosine surrogate for this RNA editing enzyme (Mizrahi et al. 2015).

Steady-state fluorescence measurements of single-stranded RNA sequences modified with thA or thI demonstrated emission differences, which unfortunately significantly diminished in a double-stranded context. Additional interference by the enzyme itself prevented real-time monitoring of the deamination process, which was resolved by adding a quenching step to the assay. Thus, hybridization with excess single-stranded DNA quenched the reaction and displaced the thA and thI-containing RNA strands, thus restoring the fluorescence difference between substrate and product. This assay, therefore, facilitates rapid fluorescent monitoring of the deamination reaction of A to I in a double-stranded RNA without the use of radiolabeled substrates, albeit not in real-time (Mizrahi et al. 2015).

Emissive mRNA constructs, incorporating thG and thA in specific codons and codon positions, have also been used to study the elongation cycle of bacterial protein translation in vitro (Liu et al. 2013, 2017). Notably, the high structural similarity facilitated the unique approach of monitoring the direct interaction of modified mRNA codons with the anticodon loops of tRNAs that could not be employed with bulkier fluorophores. Fluorescence changes detected with these responsive mRNAs facilitated the kinetic analyses of distinct ribosomal protein synthesis steps. An early event, provisionally assigned to codon/anticodon base-pairing, has been observed for the first time. Detailed analysis, focused on individual codon positions, has suggested the codon's middle position is subjected to tighter constraints, and that the mRNA/tRNA pairing occurs in a sequential manner rather than a simultaneous one (Liu et al. 2013, 2017).

thG was also utilized to fluorescently study the enzymatic base-flipping of 5-methylated cytosine (mC) residues within a DNA duplex, by the Set and Ring Associated (SRA) domain of the Ubiquitin-like containing PHD and RING Finger domains 1 (UHRF1) (Kilin et al. 2017). Along with 3HCnt (Fig. 1d), these emissive analogs, in adjacent positions to mC in a short DNA duplex, each facilitated the real-time monitoring and kinetic analysis of the binding of SRA to DNA, the base-

flipping of mC, its re-accommodation back into the strand, and the dissociation of SRA, providing new insights to the mechanism of UHRF1's activity, which is suggested to facilitate the recruitment of DNA methyl transferase 1 (DNMT1) for the replication of the DNA methylation patterns (Kilin et al. 2017).

DNA methylation in the eukaryotic genome occurs at cytosine bases by DNMTs, leading to the formation of mC mainly in a symmetrical CpG context, hence resulting in methylated residues that lie diagonally to each other. After DNA replication, hemi-methylated (HM) CpG sites are formed, where only one DNA strand is methylated; these sites are then fully methylated by DNMT1. The high replication fidelity of DNA methylation patterns, however, cannot be explained by the operation of DNMT1 alone. It is therefore proposed that UHRF1 facilitates the recruitment of DNMT1 to appropriate CpG HM sites of newly replicated DNA through preferential affinity for HM DNA over non-methylated (NM) DNA and flipping of the mC through its SRA domain (Bostick et al. 2007).

To assess this proposal, short HM and NM DNA duplexes containing thG or 3HCnt, at non-perturbing but responsive positions, facilitated the study of SRA binding and its flipping activity. Steady-state fluorescence measurements demonstrated that the flipping of mC can be monitored by the increase in QY of thG and 3HCnt. Stopped-flow measurements facilitated the kinetic analysis, suggesting that the binding of SRA proceeds through a two-step "bind-and-slide" mechanism, where the SRA first non-specifically binds to the duplex, and then slides to the CpG recognition site. The base flipping in HM duplexes was found, however, to be a much slower process, granting the UHRF1 bound to the CpG site longer time to recruit DNMT1 (Kilin et al. 2017). In addition, the motion of thG within the duplex as well as the tumbling motion of the duplex, with and without bound SRA, was monitored by Time-Resolved Fluorescence Anisotropy (TRFA), which was also used to monitor the mC flipping. TRFA measurements were in agreement with calculated values, indicating the reliability of thG as an emissive surrogate (Grytsyk et al. 2022). Notably, 2AP was unable to sense the SRA-induced base flipping of mC in the same DNA duplex, demonstrating again the high sensitivity and responsiveness of thG and 3HCnt (Kilin et al. 2017).

DNA Constructs and Conformations

A comparison between dthG and deoxy 2AP (d2Ap) replacing a specific G residue in the (−)DNA copy of the HIV-1 primer binding site, (−)PBS, an 18-mer stem-loop oligonucleotide, was undertaken (Sholokh et al. 2015). It was shown that dthG faithfully represented the conformations and dynamics of G residue, while d2AP displayed serious deficiencies. The analogs were incorporated at the G7 residue, which is part of the loop sequence itself when single-stranded, and were studied both as single-stranded and in the hybridized duplex constructs with the (+)PBS oligonucleotide. dthG remained emissive in the different DNA constructs, and its emission QY and time-resolved fluorescence decay measurements correlated well with each other as well as with the environmental changes. In contrast to d2AP-labeled

oligonucleotides, which suffered dramatic decrease in emission QYs and an abundance of dark states (non-emissive conformations with lifetimes shorter than the detection limit), only negligible fraction of "dark species" were present in the $d^{th}G$-labeled oligonucleotides highlighting its utility as a reliable fluorescent G surrogate. Additionally, within the stem-loop construct, the most emissive conformation of d2AP does not remain in the stem-loop, as the native G, but adopts an extrahelical conformation, highlighting the risk of measuring contributions from biologically irrelevant conformations (Sholokh et al. 2015).

The high QY of $d^{th}G$ in duplexes and the difference in QYs between the single-stranded stem-loop (−)PBS and the corresponding DNA duplex were further utilized to facilitate the study of the PBS annealing process with (+)PBS (Sholokh et al. 2018). Previous studies, based on the changes in FRET efficiency between two fluorescent probes attached at the 5′ and the 3′ ends of the (−)PBS, suggested that hybridization occurs either spontaneously or is mediated by protein binding. The spontaneous route was thought to occur in one step, through the short single-stranded overhangs located at the 3′ and 5′ ends of the (−)PBS and the (+)PBS, respectively, and was thought to not include interactions between the two loops. The second route was suggested to be mediated by the HIV-1 nucleocapsid protein (NC), which acts as a nucleic acid chaperone and promotes the hybridization via a loop-loop kissing intermediate in a two-step pathway (Sholokh et al. 2018).

Kinetic analyses of the fluorescent real-time monitoring of the spontaneous annealing route utilizing $d^{th}G$ or 3HCnt both suggested a two-step as opposed to the previously proposed one-step mechanism. The first step, the formation of an intermediate complex, is characterized by a quick and large fluorescence increase, which strongly suggests interactions between the loops. The second step, the conversion of the intermediate complex to the annealed product, is characterized by a slower and smaller additional increase in fluorescence. FRET-based methods, however, could not detect processes that do not significantly impact the distance between the donor and acceptor and therefore were not sensitive to loop-loop interactions (Sholokh et al. 2018).

Somewhat surprisingly, the non-isomorphic universal nucleobase 3HCnt had an advantage over ^{th}G in studying the NC-mediated annealing. ^{th}G was restricted to the one guanosine position found in the loop and did not show differences in fluorescence intensity between the NC-bound single strand and the annealed double-stranded construct. In contrast, the universal and responsive 3HCnt was found to be tolerated at one position, out of several tested, with little to no perturbation, and was used to fluorescently monitor the annealing process induced by NC. Kinetic parameters were similar to the results obtained by the FRET-based method. This example highlights the need to explore multiple probes and constructs to secure a complete picture of complex processes (Sholokh et al. 2018).

^{th}G was also used to monitor B to Z transitions, by either directly monitoring its fluorescence changes (Park et al. 2014) or by creating a FRET pair (Han et al. 2017). The latter was also used to monitor changes in large DNA constructs such as nucleosomes (Han et al. 2018). It was initially found that ^{th}G stabilizes the B-form, likely due to its preference of the anti-conformation, as very high salt

concentrations were required to induce transition to the Z form (Park et al. 2014). Incorporation of 8-methylguanine to the thG-labeled DNA oligonucleotide, as a Z-DNA stabilizing unit, facilitated the B to Z transition induced by either increasing the ionic strength or by adding Zαβ, a Z-DNA binding protein (Park et al. 2014). It was subsequently demonstrated that incorporation of 2′-methoxy-thG (2'-OMe-thG) into DNA also facilitated the B to Z transition, excluding the need to use 8-methylguanine (Yamamoto et al. 2015). In both cases thG was found responsive to global changes, resulting in a strong fluorescent enhancement in Z- over B-form DNA duplexes (Park et al. 2014; Yamamoto et al. 2015).

B to Z transitions were further explored by creating a FRET pair between dthG as a donor and 1,3-diaza-2-oxophenothiazine (tC) (Fig. 1b, Engman et al. 2004), an extended fluorescent deoxycytidine analog, as the acceptor (Han et al. 2017). The rigid positioning of the D/A in such constructs enabled to control both the distance (R_{DA}) and the orientation factor ($\boldsymbol{\kappa}^2$) of the FRET pair, as opposed to the common approach, where D/A are attached through flexible linkers allowing free rotation of the fluorophores; therefore $\boldsymbol{\kappa}^2$ is assumed to be 2/3. Among several D/A incorporation distances evaluated in a hairpin-forming oligodeoxynucleotide, an optimal D/A distance was found where the FRET efficiency from 2'-OMe-thG to tC gradually decreased upon transition between B- and Z-forms (induced by increasing salt concentrations). A major contribution to the appreciable decrease in FRET efficiency, which included a hypsochromic shift in the emission maximum and a hyperchromic effect on the fluorescence intensity, was attributed to the orientation factor (Han et al. 2017).

This FRET pair was further utilized within nucleosome constructs consisting of 145 bp (Han et al. 2018). PCR was used for oligonucleotide synthesis with the emissive analogs present in the PCR primers. Two nucleosomes were constructed, with different D/A distances. As expected, different FRET efficiencies were measured for the distinct D/A constructs. A significant impact of the orientation factor was again suggested to account for the observed difference in FRET efficiencies. This proof of concept demonstrates the potential of using this FRET pair to study conformational dynamics in genetic processes (Han et al. 2018).

Conclusions

Isomorphic fluorescent nucleoside analogs, by maintaining similar structure to their native analogs while possessing useful photophysical properties, allow researchers to study and fluorescently monitor processes involving their non-emissive natural counterparts. This chapter described their applications, advantages over other tools, including other fluorescence-based methods, and their limitations.

Due to the intrinsic fluorescence possessed by isomorphic fluorescent nucleosides, enzymatic reactions generate a new, distinct emissive molecule. A change in the photophysical properties can therefore be monitored by changes in fluorescence intensity, fluorescence lifetime, emission wavelength, fluorescence anisotropy, or other parameters. Additionally, information regarding the enzyme's tolerance for

structural modifications and indications for the reaction's mechanism can be indirectly obtained. These photophysical features can also facilitate the development of fluorescent-based assays for monitoring enzymatic activity or for inhibitor screening, which are typically amendable for conversation to high-throughput screening setups.

The isomorphic nature of the analogs and their faithful representation of the canonical nucleosides enable their sequence-specific incorporation into RNA and DNA oligonucleotides. Examples of fluorescently monitoring oligonucleotides' annealing process or base-flipping, discussed in this chapter, emphasize how sensitive and responsive these analogs can be to changes in their microenvironment.

Since emissive isomorphic analogs do not function as a simple fluorescent tag, the specific biochemical constraints constraints and the limitations of the and the limitations of the probes themselves need to be carefully evaluated. Certain possible limitations include structural/folding perturbations to the construct in question (as in the case of the HH16 ribozyme containing multiple isomorphic replacements), population of biologically irrelevant conformation (as possible in the case of 2AP within a DNA oligonucleotide), or coincidental lack of fluorescence signal change. These limitations cannot always be predicted; therefore, the examination use of more than one probe can frequently be beneficial.

A lower level of isofunctionality is not always a disadvantage, as it could result in extended reaction times, which can frequently be useful for kinetics studies. In the case of the thA-incorporated mRNA utilized to study the elongation process of protein translation, lower isofunctionality shed light on the pairing pathway between the mRNA and the tRNA's anticodon. In addition, lower isofunctionality of CDN analogs potentially granted them longer cellular residency time that enhanced their immunomodulatory effect.

Numerous other processes involving nucleosides, nucleoside-based cofactors, and nucleic acids await to be studied. Recent reports of cellular RNA condensates (Roden and Gladfelter 2021), small RNAs modified with N-glycans (Flynn et al. 2021), and development of RNA therapeutics (Kim 2022) can all benefit from utilizing isomorphic fluorescent nucleoside analogs. We hope this chapter would inspire new directions and expansion of the biological systems explored, as well as the development of new and further improved emissive isomorphic nucleoside analogs.

References

Adamek RN, Ludford P, Duggan SM et al (2020) Identification of adenosine deaminase inhibitors by metal-binding pharmacophore screening. Chem Med Chem 15:2151–2156. https://doi.org/10.1002/cmdc.202000271

Barrio JR, Secrist JA, Leonard NJ (1972) A fluorescent analog of nicotinamide adenine dinucleotide. Proc Natl Acad Sci U S A 69:2039–2042. https://doi.org/10.1073/pnas.69.8.2039

Bostick M, Kim JK, Estève P-O et al (2007) UHRF1 plays a role in maintaining DNA methylation in mammalian cells. Science 317(80):1760–1764. https://doi.org/10.1126/science.1147939

Bucardo MS, Wu Y, Ludford PT et al (2021) Real-time monitoring of human guanine deaminase activity by an emissive guanine Analog. ACS Chem Biol 16:1208–1214. https://doi.org/10.1021/acschembio.1c00232

Coleman RS, Madaras ML (1998) Synthesis of a novel coumarin C-riboside as a photophysical probe of oligonucleotide dynamics. J Org Chem 63:5700–5703. https://doi.org/10.1021/jo980478+

Cong D, Li Y, Ludford PT, Tor Y (2022) Isomorphic fluorescent nucleosides facilitate real-time monitoring of RNA Depurination by ribosome inactivating proteins. Chem Eur J 28. https://doi.org/10.1002/chem.202200994

Crespo-Hernández CE, Cohen B, Hare PM, Kohler B (2004) Ultrafast excited-state dynamics in nucleic acids. Chem Rev 104:1977–2019. https://doi.org/10.1021/cr0206770

Da Costa CP, Fedor MJ, Scott LG (2007) 8-Azaguanine reporter of purine ionization states in structured RNAs. J Am Chem Soc 129:3426–3432. https://doi.org/10.1021/ja067699e

Dodd D, Hudson R (2009) Intrinsically fluorescent base-discriminating nucleoside analogs. Mini Rev Org Chem 6:378–391. https://doi.org/10.2174/157019309789371659

Dziuba D (2022) Environmentally sensitive fluorescent nucleoside analogues as probes for nucleic acid – protein interactions: molecular design and biosensing applications. Methods Appl Fluoresc 10. https://doi.org/10.1088/2050-6120/ac7bd8

Dziuba D, Postupalenko VY, Spadafora M et al (2012) A universal nucleoside with strong two-band switchable fluorescence and sensitivity to the environment for investigating DNA interactions. J Am Chem Soc 134:10209–10213. https://doi.org/10.1021/ja3030388

Dziuba D, Didier P, Ciaco S et al (2021) Fundamental photophysics of isomorphic and expanded fluorescent nucleoside analogues. Chem Soc Rev 50:7062–7107. https://doi.org/10.1039/d1cs00194a

Engman KC, Sandin P, Osborne S et al (2004) DNA adopts normal B-form upon incorporation of highly flourescent DNA base analogue tC: NMR structure and UV-vis spectroscopy characterization. Nucleic Acids Res 32:5087–5095. https://doi.org/10.1093/nar/gkh844

Feldmann J, Li Y, Tor Y (2019) Emissive synthetic cofactors: a highly responsive NAD + analogue reveals biomolecular recognition features. Chem Eur J 25:4379–4389. https://doi.org/10.1002/chem.201805520

Fillion A, Franco Pinto J, Granzhan A (2022) Harnessing an emissive guanine surrogate to design small-molecule fluorescent chemosensors of O 6-methylguanine-DNA-methyltransferase (MGMT). Org Biomol Chem 20:1888–1892. https://doi.org/10.1039/d2ob00208f

Flynn RA, Pedram K, Malaker SA et al (2021) Small RNAs are modified with N-glycans and displayed on the surface of living cells. Cell 184:3109–3124.e22. https://doi.org/10.1016/j.cell.2021.04.023

Gaied NB, Glasser N, Ramalanjaona N, et al (2005) 8-Vinyl-Deoxyadenosine, an Alternative Fluorescent Nucleoside Analog To 2′-Deoxyribosyl-2-Aminopurine With Improved Properties. Nucleic Acids Res 33:1031–1039. https://doi.org/10.1093/nar/gki253

Godde F, Toulmé JJ, Moreau S (1998) Benzoquinazoline derivatives as substitutes for thymine in nucleic acid complexes. Use of fluorescence emission of benzo[g]quinazoline-2, 4-(1H, 3H)-dione in probing duplex and triplex formation. Biochemistry 37:13765–13775. https://doi.org/10.1021/bi9811967

Grytsyk N, Richert L, Didier P et al (2022) Thienoguanosine, a unique non-perturbing reporter for investigating rotational dynamics of DNA duplexes and their complexes with proteins. Int J Biol Macromol 213:210–225. https://doi.org/10.1016/j.ijbiomac.2022.05.162

Gustavsson T, Markovitsi D (2021) Fundamentals of the intrinsic DNA fluorescence. Acc Chem Res 54:1226–1235. https://doi.org/10.1021/acs.accounts.0c00603

Hallé F, Fin A, Rovira AR, Tor Y (2018) Emissive synthetic cofactors: enzymatic interconversions of tzA analogues of ATP, NAD^+, NADH, $NADP^+$, and NADPH. Angew Chemie Int Ed 57:1087–1090. https://doi.org/10.1002/anie.201711935

Han JH, Yamamoto S, Park S, Sugiyama H (2017) Development of a vivid FRET system based on a highly emissive dG–dC analogue pair. Chem A Eur J 23:7607–7613. https://doi.org/10.1002/chem.201701118

Han JH, Park S, Hashiya F, Sugiyama H (2018) Approach to the investigation of nucleosome structure by using the highly emissive nucleobase thdG–tC FRET pair. Chem Eur J 24: 17091–17095. https://doi.org/10.1002/chem.201803382

Hardman SJO, Botchway SW, Thompson KC (2008) Evidence for a nonbase stacking effect for the environment-sensitive fluorescent base pyrrolocytosine – comparison with 2-aminopurine. Photochem Photobiol 84:1473–1479. https://doi.org/10.1111/j.1751-1097.2008.00368.x

Hawkins ME (2001) Fluorescent pteridine nucleoside analogs: a window on DNA interactions. Cell Biochem Biophys 34:257–281. https://doi.org/10.1385/CBB:34:2:257

Jones AC, Neely RK (2015) 2-aminopurine as a fluorescent probe of DNA conformation and the DNA-enzyme interface. Q Rev Biophys 48:244–279. https://doi.org/10.1017/S0033583514000158

Kilin V, Gavvala K, Barthes NPF et al (2017) Dynamics of methylated cytosine flipping by UHRF1. J Am Chem Soc 139:2520–2528. https://doi.org/10.1021/jacs.7b00154

Kim YK (2022) RNA therapy: rich history, various applications and unlimited future prospects. Exp Mol Med 54:455–465. https://doi.org/10.1038/s12276-022-00757-5

Leonard NJ, Sprecker MA, Morrice AG (1976) Defined dimensional changes in enzyme substrates and cofactors. Synthesis of lin-benzoadenosine and enzymic evaluation of derivatives of the benzopurines. J Am Chem Soc 98:3987–3994. https://doi.org/10.1021/ja00429a040

Li Y, Fin A, McCoy L, Tor Y (2017) Polymerase-mediated site-specific incorporation of a synthetic fluorescent isomorphic G surrogate into RNA. Angew Chemie Int Ed 56:1303–1307. https://doi.org/10.1002/anie.201609327

Li Y, Fin A, Rovira AR et al (2020a) Tuning the innate immune response to cyclic dinucleotides by using atomic mutagenesis. Chem Bio Chem 21:2595–2598. https://doi.org/10.1002/cbic.202000162

Li Y, Ludford PT, Fin A et al (2020b) Enzymatic syntheses and applications of fluorescent cyclic dinucleotides. Chem Eur J 26:6076–6084. https://doi.org/10.1002/chem.202001194

Liu W, Shin D, Tor Y, Cooperman BS (2013) Monitoring translation with modified mRNAs strategically labeled with isomorphic fluorescent guanosine mimetics. ACS Chem Biol 8: 2017–2023. https://doi.org/10.1021/cb400256h

Liu W, Shin D, Ng M et al (2017) Stringent nucleotide recognition by the ribosome at the middle codon position. Molecules 22:1–12. https://doi.org/10.3390/molecules22091427

Long DM, Uhlenbeck OC (1994) Kinetic characterization of intramolecular and intermolecular hammerhead RNAs with stem II deletions. Proc Natl Acad Sci U S A 91:6977–6981. https://doi.org/10.1073/pnas.91.15.6977

Ludford PT, Tor Y (2020) Ascertaining the activity and inhibition of adenosine deaminase via fluorescence-based assays. In: Methods in enzymology, 1st edn. Elsevier Inc., pp 71–90

Ludford PT, Rovira AR, Fin A, Tor Y (2019) Fluorescing Isofunctional Ribonucleosides: assessing adenosine deaminase activity and inhibition. Chem Bio Chem 20:718–726. https://doi.org/10.1002/cbic.201800665

Ludford PT, Li Y, Yang S, Tor Y (2021) Cytidine deaminase can deaminate fused pyrimidine ribonucleosides. Org Biomol Chem 19:6237–6243. https://doi.org/10.1039/d1ob00705j

Ludford PT, Yang S, Bucardo MS, Tor Y (2022) A new variant of emissive RNA alphabets. Chem Eur J 28:6–11. https://doi.org/10.1002/chem.202104472

Martinez-Fernandez L, Gustavsson T, Diederichsen U, Improta R (2020) Excited state dynamics of 8-vinyldeoxyguanosine in aqueous solution studied by time-resolved fluorescence spectroscopy and quantum mechanical calculations. Molecules 25, 824. https://doi.org/10.3390/molecules25040824

McCoy LS, Shin D, Tor Y (2014) Isomorphic emissive GTP surrogate facilitates initiation and elongation of in vitro transcription reactions. J Am Chem Soc 136:15176–15184. https://doi.org/10.1021/ja5039227

Mély Y, Kuchlyan J, Martinez-Fernandez L et al (2020) What makes thienoguanosine an outstanding fluorescent DNA probe? J Am Chem Soc 142:16999–17014. https://doi.org/10.1021/jacs.0c06165

Micozzi D, Carpi FM, Pucciarelli S et al (2014) Human cytidine deaminase: a biochemical characterization of its naturally occurring variants. Int J Biol Macromol 63:64–74. https://doi.org/10.1016/j.ijbiomac.2013.10.029

Mizrahi RA, Shin D, Sinkeldam RW et al (2015) A fluorescent adenosine analogue as a substrate for an A-to-I RNA editing enzyme. Angew Chemie Int Ed 54:8713–8716. https://doi.org/10.1002/anie.201502070

Navas LE, Carnero A (2021) NAD+ metabolism, stemness, the immune response, and cancer. Signal Transduct Target Ther 6,2. https://doi.org/10.1038/s41392-020-00354-w

Okamoto A, Tanaka K, Fukuta T, Saito I (2003) Design of base-discriminating fluorescent nucleoside and its application to T/C SNP typing. J Am Chem Soc 125:9296–9297. https://doi.org/10.1021/ja035408l

Okamoto A, Tanaka K, Fukuta T, Saito I (2004) Cytosine detection by a fluorescein-labeled probe containing base-discriminating fluorescent nucleobase. Chem Bio Chem 5:958–963. https://doi.org/10.1002/cbic.200400010

Okamoto A, Saito Y, Saito I (2005) Design of base-discriminating fluorescent nucleosides. J Photochem Photobiol C: Photochem Rev 6:108–122. https://doi.org/10.1016/j.jphotochemrev.2005.07.002

Park S, Otomo H, Zheng L, Sugiyama H (2014) Highly emissive deoxyguanosine analogue capable of direct visualization of B-Z transition. Chem Commun 50:1573–1575. https://doi.org/10.1039/c3cc48297a

Rist M, Marino J (2002) Fluorescent Nucleotide Base Analogs as probes of nucleic acid structure, dynamics and interactions. Curr Org Chem 6:775–793. https://doi.org/10.2174/1385272023373914

Roden C, Gladfelter AS (2021) RNA contributions to the form and function of biomolecular condensates. Nat Rev Mol Cell Biol 22:183–195. https://doi.org/10.1038/s41580-020-0264-6

Rovira AR, Fin A, Tor Y (2015) Chemical mutagenesis of an emissive RNA alphabet. J Am Chem Soc 137:14602–14605. https://doi.org/10.1021/jacs.5b10420

Rovira AR, Fin A, Tor Y (2017a) Expanding a fluorescent RNA alphabet: synthesis, photophysics and utility of isothiazole-derived purine nucleoside surrogates. Chem Sci 8:2983–2993. https://doi.org/10.1039/C6SC05354H

Rovira AR, Fin A, Tor Y (2017b) Emissive synthetic cofactors: an isomorphic, isofunctional, and responsive NAD+ analogue. J Am Chem Soc 139:15556–15559. https://doi.org/10.1021/jacs.7b05852

Saito Y, Hudson RHE (2018) Base-modified fluorescent purine nucleosides and nucleotides for use in oligonucleotide probes. J Photochem Photobiol C: Photochem Rev 36:48–73. https://doi.org/10.1016/j.jphotochemrev.2018.07.001

Saito Y, Koda M, Shinohara Y, Saito I (2011) Synthesis and photophysical properties of 8-arylbutadienyl 2′-deoxyguanosines. Tetrahedron Lett 52:491–494. https://doi.org/10.1016/j.tetlet.2010.11.053

Secrist JA, Barrio JR, Leonard NJ (1972) A fluorescent modification of adenosine triphosphate with activity in enzyme systems: 1, N 6 -ethenoadenosine triphosphate. Science 175(80):646–647. https://doi.org/10.1126/science.175.4022.646

Shin D, Sinkeldam RW, Tor Y (2011) Emissive RNA alphabet. J Am Chem Soc 133:14912–14915. https://doi.org/10.1021/ja206095a

Sholokh M, Sharma R, Shin D et al (2015) Conquering 2-aminopurines deficiencies: highly emissive isomorphic guanosine surrogate faithfully monitors guanosine conformation and dynamics in DNA. J Am Chem Soc 137:3185–3188. https://doi.org/10.1021/ja513107r

Sholokh M, Sharma R, Grytsyk N et al (2018) Environmentally sensitive fluorescent nucleoside analogues for surveying dynamic interconversions of nucleic acid structures. Chem Eur J 24:13850–13861. https://doi.org/10.1002/chem.201802297

Sinkeldam RW, Greco NJ, Tor Y (2010) Fluorescent analogs of biomolecular building blocks: design, properties, and applications. Chem Rev 110:2579–2619. https://doi.org/10.1021/cr900301e

Sinkeldam RW, McCoy LS, Shin D, Tor Y (2013) Enzymatic interconversion of isomorphic fluorescent nucleosides: adenosine deaminase transforms an adenosine analogue into an inosine analogue. Angew Chemie Int Ed 52:14026–14030. https://doi.org/10.1002/anie.201307064

Tor Y, Del Valle S, Jaramillo D et al (2007) Designing new isomorphic fluorescent nucleobase analogues: the thieno [3,2-d] pyrimidine core. Tetrahedron 63:3608–3614. https://doi.org/10.1016/j.tet.2007.01.075

Veth S, Fuchs A, Özdemir D et al (2022) Chemical synthesis of the fluorescent, cyclic dinucleotides cthGAMP. Chembiochem 23:6–11. https://doi.org/10.1002/cbic.202200005

Vranken C, Fin A, Tufar P et al (2016) Chemoenzymatic synthesis and utilization of a SAM analog with an isomorphic nucleobase. Org Biomol Chem 14:6189–6192. https://doi.org/10.1039/c6ob00844e

Wierzchowski J, Antosiewicz JM, Shugar D (2014) 8-Azapurines as isosteric purine fluorescent probes for nucleic acid and enzymatic research. Mol BioSyst 10:2756–2774. https://doi.org/10.1039/c4mb00233d

Wilhelmsson LM (2010) Fluorescent nucleic acid base analogues. Q Rev Biophys 43:159–183. https://doi.org/10.1017/S0033583510000090

Wilson JN, Kool ET (2006) Fluorescent DNA base replacements: reporters and sensors for biological systems. Org Biomol Chem 4:4265–4274. https://doi.org/10.1039/b612284c

Xu W, Chan KM, Kool ET (2017) Fluorescent nucleobases as tools for studying DNA and RNA. Nat Chem 9:1043–1055. https://doi.org/10.1038/NCHEM.2859

Yamamoto S, Park S, Sugiyama H (2015) Development of a visible nanothermometer with a highly emissive 2′-O-methylated guanosine analogue. RSC Adv 5:104601–104605. https://doi.org/10.1039/c5ra24756j

Ying W (2008) NAD+/NADH and NADP+/NADPH in cellular functions and cell death: regulation and biological consequences. Antioxidants Redox Signal 10:179–206. https://doi.org/10.1089/ars.2007.1672

Young JS, Jin HR, Byeang HK (2005) Quencher-free, end-stacking oligonucleotides for probing single-base mismatches in DNA. Org Lett 7:4931–4933. https://doi.org/10.1021/ol0518582

Yu H, Chao J, Patek D et al (1994) Cyanine dye dUTP analogs for enzymatic labeling of DNA probes. Nucleic Acids Res 22:3226–3232. https://doi.org/10.1093/nar/22.15.3226

Zhou J, Zheng Y, Roembke BT et al (2017) Fluorescent analogs of cyclic and linear dinucleotides as phosphodiesterase and oligoribonuclease activity probes. RSC Adv 7:5421–5426. https://doi.org/10.1039/c6ra25394f